PROPERTIES OF MAGNETOSPHERIC HIGH ENERGY PARTICLES BASED ON ANALYSIS OF DATA FROM STEP-F AND SPHINX INSTRUMENTS ONBOARD THE "CORONAS-PHOTON" SATELLITE

O. Dudnik[1,2], J. Sylwester[3], P. Podgórski[3]

[1] Institute of Radio Astronomy, National Academy of Sciences of Ukraine (IRA NASU)
[2] V.N. Karazin Kharkiv National University, Ministry of Education and Science of Ukraine (KhNU)
[3] Solar Physics Division, Space Research Centre, Polish Academy of Sciences, Poland (SRC PAS)

The SphinX solar photometer in X-rays as the recorder of high energy charged particles

The satellite telescope of electrons and protons STEP-F, which was designed and manufactured by the KhNU, was placed aboard the "CORONAS-Photon". The instrument was designed to study distributions of high energy charged particles under the Earth radiation belts [1]. Due to substantial geometry factor of this telescope, and thanks to a high ratio of signal to the noise of its semiconductor detectors as well as due to some other unique characteristics new scientific results were obtained [2].

The SphinX solar photometer in X-rays was designed and manufactured at the Solar Physics Division of the SRC PAS. The instrument was the part of the scientific payload of the CORONAS-Photon satellite [3]. During data processing obtained from this instrument it was found that the count rates of spectrophotometer sensors in high energy channels are substantial even during passages over the night portions of the orbit. The count rate increased sharply with the satellite passage of regions of the Brazilian Magnetic Anomaly (BMA ≡ South Atlantic Anomaly) and radiation belts (RBs) suggesting a response of SphinX detectors to presence of ambient high energy particles.

The sensor unit STEP-FD of the STEP-F instrument was located in close proximity to the SphinX. This enabled us to perform a joint analysis of data from the particle detection channels of the SphinX spectrophotometer and STEP-F channels recording electrons and protons of intermediate energies.

In SphinX spectrophotometer, four silicon PIN photodiodes served as sensors. These detectors were equipped with independent processing electronics. Each sensor had 500 μm thickness Si crystal intended for detection of X-rays. The crystal active area was however different. Detectors were equipped with 12.5 μm beryllium foils allowing to pass the higher energy X-rays, above approximately 1 keV. Note, The EUV solar radiation was stopped by the thin double sided aluminized mylar foil mounted on the instrument entrance window. *Det2* sensor of active area $S_2 = 0.111$ cm^2 was covered in addition by a double tantalum plate with a total thickness of 400 μm while maintaining an open window of $S_{2o} = 4.9\times10^{-3}$ cm^2 for registering X-ray bursts from solar flares of medium to high class.

The energy resolution of the detector *Det1* was about 0.4 keV over the entire registration range $\Delta E = 0—15$ keV covered by 256 energy channels of the spectrometric analog-to-digital converter. Herewith the minimum energy threshold for signal detection coming from the sensor *Det1* with the active area of $S_1 = 0.215$ cm^2 was set as corresponding to the energy of 1.1 keV. Respective energy threshold for the *Det2* detector was set at the level of 0.85 keV. The view axis of the three SphinX spectrophotometric detectors was directed along the OZ axis of the spacecraft, which was stabilized during the experiment to the centre of the Sun direction. The fields of view of *Det1* and *Det2* detectors were 1.94×1.94° and 1.72×1.72° respectively centered along this axis. In the following analysis, the data from the 254th and 255th spectrometer energy channels of *Det1* and *Det2* sensors were used as all detector events corresponding to energies higher than approximately 15 keV were directed to these last bins.

The STEP-F satellite telescope of electrons and protons comprised the STEP-FD sensor unit and the digital information processing unit STEP-FE, which was located inside the sealed chamber of the CORONAS-Photon spacecraft. The detector head of the STEP-FD sensor unit contain of two identical silicon position-sensitive matrix detectors D1 and

D2, and two scintillation detectors based on CsI(Tl) monocrystals. Particle-related luminescence splashes inside the scintillators were monitored by a large area silicon photodiodes interacting with the D3 detection layer, and by the vacuum photomultiplier interacting with the D4 detector. The latter detector, recorded the secondary γ-quanta of intermediate energies from the interaction of primary electrons with three layers of detectors and their holders consisting of D3 (13 mm thickness CsI(Tl)) and detectors D1 and D2 (of the total Si thickness of 760 μm), as well as the constructional materials of aluminum. The total angle of view of the telescope was 108×108° for low energy particles and 98×98° for high energy particles. The axis of the telescope was at the right angle to the OZ line directed to the Sun. Effective areas of each of the semiconductor detectors were 17 cm^2, and for the scintillation crystal detectors they were of 36 cm^2 and 49 cm^2 respectively. In the Table some important characteristics of STEP-F and SphinX detectors and the respective energy ranges used in common data analysis are presented.

Sensitivity of SphinX detectors to mixed particle background

In order to find the particle types and energy ranges that contribute to *Det1* and *Det2* detector signals, we have performed a common data analysis at the time of a weak geomagnetic storm (D_{st} = –26 nT) which took place on 8th May 2009 [4]. At the time of RBs and BMA crossings, we have found that *Det1* and *Det2* responses coincided with electron flux enhancements seen by STEP-F detectors. Count rates on the *Det1* were almost always higher than count rates on *Det2* by a factor of ~5÷10. The exception were crossing of the BMA, where the count rate measured by both sensors were of similar magnitude. Close to the BMA center the intensity of particle count rate in the *Det2* channel becomes even greater than the one sensed in *Det1* channel. The latter indicates for different sensitivity of *Det1 and Det2* sensor readouts to a change of the primary particle spectra in particular zones of the inner magnetosphere.

Sufficiently high count rates of *Det1 and Det2* detectors taking observations within a very narrow fields of view, the observed disparity between ratio of their signals and the difference of their active areas indicates for presence of an additional component in their recorded signal, arising from a larger solid angle. The low energy secondary γ-quanta generated as a result of primary electron interactions with the detector head construction materials, entire TESIS instrument complex, and the spacecraft itself, might be responsible for such a component. Thus, we conclude that *Det1* and *Det2* detectors of the SphinX instrument are sensitive to a mixture electron ambient populations namely to the low energy electrons and the secondary γ-radiation, generated by primary electrons of higher energies. The latter circumstance allowed us to invoke the concept of effective lower energy thresholds for electron detection (E_{thr1} and E_{thr2} respectively) by *Det1* and *Det2* detectors, respectively. Respective values of these thresholds can vary depending on the energy profile of the primary electron energy spectrum.

Effective energies of trapped electrons, registered by STEP-F and SphinX detectors inside BMA

Trapped electrons were detected within the BMA region at the orbit altitude (~550 km) of the "CORONAS-Photon" satellite. In order to analyze the distributions of particle fluxes trough the L-shells, when crossing of the BMA regions, we analyzed ascending path of the fifth orbits of the day. In Fig. 1 we present an example of derived particle flux density distribu-

Designations and characteristics of the recording channels of the SphinX and STEP-F instruments

Instrument	SphinX		STEP-F			
Detector name & channel	*Det1*	*Det2*	D1e	D1p	D2e	D4e
Recorded particle energy range, MeV	—	—	Electrons ΔE_e = = 0.18—0.51 + + protons ΔE_p = 3.5—3.7	Protons ΔE_p = = 3.7—7.4 + + electrons ΔE_e = 0.55—0.95	Electrons ΔE_e = = 0.35—0.95	Secondary γ-radiation from electrons with $E_e \geq$ 0.6—0.8
Detector type	Si PIN	Si PIN	Si PIN	Si PIN	Si PIN	CsI(Tl) + vacuum photomultiplier
Detector thickness, μm	500	500	380	380	380	5000
Active area, $см^2$	0.215*	0.111*	17	17	17	49

* The active area of the detector for particle detection is limited by detectors' internal collimator. For X-ray measurements the effective area has another value related with presence of external collimator.

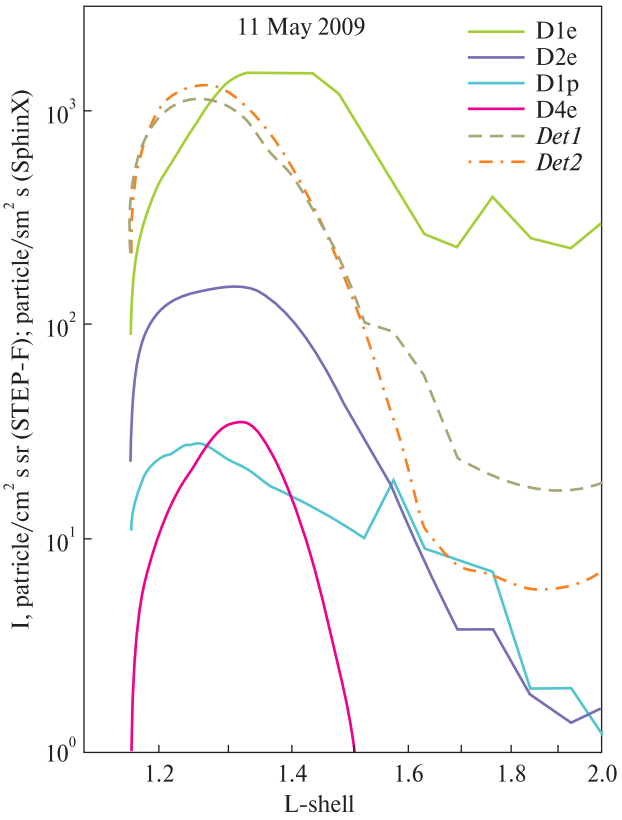

Fig. 1. The particle intensity distribution through L-shells within the BMA recorded on the fifth (of the day) ascending node of the satellite orbit for May 11, 2009. Particle fluxes for the SphinX device are not normalized over solid angle

tions for the four energy channels of the STEP-F instrument and for both SphinX detectors as recorded on 11 May 2009. Clearly seen is the changing ratio of count rates between *Det1* and *Det2* detectors when passing from lower values of L ~ 1.25 to L ~ 1.85. A much steeper decrease in count rates of *Det2* channel at higher L-shells indicates for a significant change of the energy spectrum of primary electrons related to a fast decrease of high energy tail in the electron population. This is confirmed by a changing shape of D1e channel intensity profile between L-shells from L ~ 1.5 to L ~ 1.9, a sharp decrease of electron fluxes in D2e and D1p channels within these limits of the Mc-Ilwain parameter, and the fast drop of counts in the D4e channel, related to a decrease of secondary γ-radiation.

The analysis of location of maxima of particle intensities along the L-shell axis, as averaged for 14 days within the period 1–14 May, 2009, allowed us to determine the values of E_{thr1} and E_{thr2} for the SphinX *Det1* and *Det2* detectors. It was also possible to determine the effective recording energy for the STEP-F E_{D4e} detector. Herewith, relationships of the Earth's magnetic field to the magnetic field at the geomagnetic equator for the period considered possessed the values of $B/B_0 \approx 1.2 \div 1.6$. In Fig. 2 we present respective dependence of L-shell values, at which maximum particle fluxes were observed, on the electron energy bound to respective D2e and D1p channels of the STEP-F device.

It is seen from Fig. 2 that the values of E_{thr1} and E_{thr2} are very close to each other, and are ~500 keV and ~475 keV for *Det1* and *Det2* respectively. However, it is observed that the dispersion of these values was quite large and connected not only with a low statistics (covering 14 days only), but also to some extent with the diurnal displacement of the satellite in the longitude at the fixed latitude relative to the initial time. These effects caused the changing slightly observed electron spectrum from day to day.

From the graph presented in Fig. 2 the value of $E_{D4e} \approx 335$ keV was determined as well. However, this E_{D4e} value has been observed changing from day to day too in the range between 230 and 350 keV in the observed period within 1st and 14th May of 2009. Lower threshold values of the electron detection energy in the last detector of the STEP-FD telescopic system as compared with respective E_{thr1} and E_{thr2} of

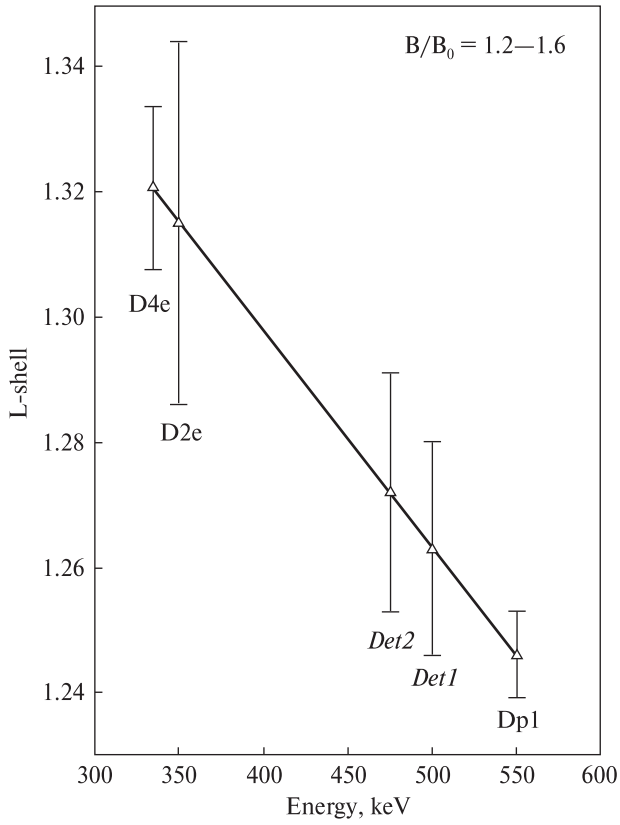

Fig. 2. The dependence of L-shell values, at which maxima of particle fluxes have been seen during the BMA passes plotted against their energy. The L-values of maxima were determined for ascending nodes on fifth orbits of a day in the period between 1 and 14 May, 2009

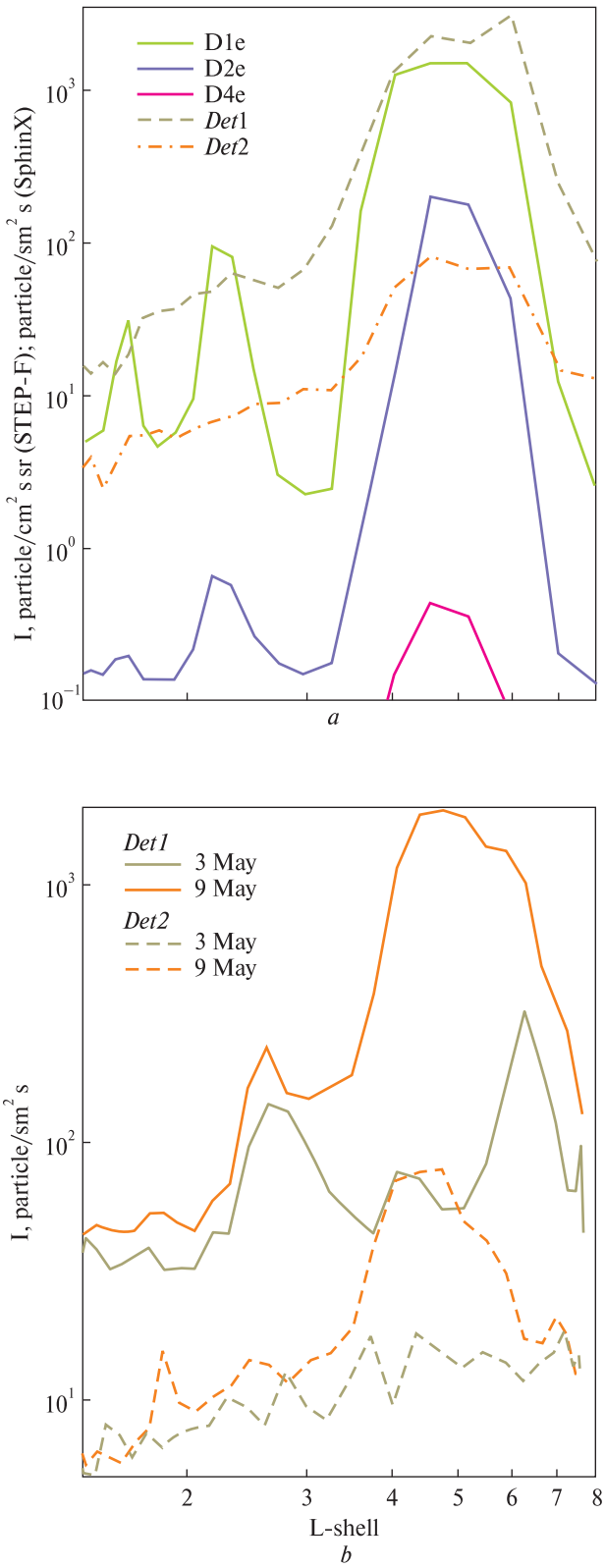

Fig. 3. (*a*) The distribution of particle fluxes over L-shells in RBs in the northern hemisphere as seen on the ninth (of the day) ascending portion of the spacecraft orbit in five channels of both instruments on 8th May 2009; (*b*) the distribution over L-shells of the particle fluxes in RBs in the southern hemisphere as recorded on the first descending node of the spacecraft orbit in the *Det1* and *Det2* channels on 3rd and 9th May 2009

the SphinX spectrophotometer, are due to the high efficiency of registration by STEP-F scintillation detector, related with its large active area as well as its very low photomultiplier tube noise.

Analysis of radiation belts characteristics outside the BMA based on STEP-F and SphinX data

For "CORONAS-Photon" orbits not touching the BMA regions it is possible to study behavior of radiation belts throughout entire mission. Notable discrepancies of maximum count rate occurrences in the RBs both by time and by the L-shells have been observed between records obtained from both instruments except for the days of the maximum and early stage of the geomagnetic storm recovery phase on May 8—10, 2009 when relative distributions of particle intensities by L-shells in the outer RB were very similar for both instruments. Fig. 3 shows the distributions of particle intensity in recording channels of both instruments during transit of the northern hemisphere on 8 May 2009 (Fig. 3, *a*) and changes of the measured signal in *Det1* and *Det2* of SphinX in the southern hemisphere on 3rd and 9th May 2009 (Fig. 3, *b*). The inspection of Fig. 3a reveals that the STEP-F device observed presence of three electron belts in two energy ranges. The electron population of the third "additional" belt is characterized by a softer energy spectrum as its corresponding intensity drops rather sharply at $E > 0.55$ MeV [5—7].

The SphinX spectrophotometer might record the innermost RBs too, as a substantial steepening of the particle intensity at $L = 1.6$ and its decline at $2.5 < L < 2.8$ in the *Det1* channel is noticeable; however the sensitivity of the instrument was not sufficient to reveal the presence of the innermost RBs confidently [8]. The second reason by which SphinX have not seen inner RBs directly could be non-overlapping fields of views of both instruments. Another factor could be a narrow-band character of electron distribution function in the innermost belt. As concerns particle intensity distribution over L-shells in the southern hemisphere, SphinX observed the innermost RB in both channels for 3rd and 9th May of 2009 (Fig. 3, *b*). Presence of inner Van Allen belt on the *Det1* records can be seen both during the geomagnetically quiet period, and during the initial phase of the geomagnetic storm recovery stage. It also can be seen that the count rates for *Det2* channel and its sensitivity to changes in particle fluxes were significantly lower than for *Det1* channel. This again confirms the conclusion that *Det2* channel recorded a higher energy portion of the electron spectrum.

Evidence of presence of the three electron radiation belts using STEP-F measurements

The specific feature of "CORONAS-Photon" satellite orbit was its passing the same near Earth space environment every 15 orbit pass, i.e. after approximately every 24 elapsed hours. As far as the distribution of high energy particle fluxes inside the Earth magnetosphere depends on the latitude, longitude and the height of the satellite it's usefully to compare the intensities in the same or very close spatial locations at different time intervals. As the satellite orbit was very close to circular, these requirements are restricted by two parameters only: by latitude and longitude. For the case analyzed the same areas which the satellite flown periodically came in every 24 hours. The longitude drift of the orbit was not more than 2.5° every 24 hours. By combining the data recorded over the same area from several passes we could obtain the possibility to trace electron fluxes dynamics. Fig. 4 demonstrates the time dependence of STEP-F signal due to presence of electrons with energies from the range $\Delta E_e = 0.18—0.51$ MeV in the period from 1 till 31 May 2009 as recorded on the ninth orbit pass of the day (counted in Universal Time). From bottom to top signal variations are plotted from 1st to 48th minutes of satellite flight as measured from the moment of the maximal latitude reached by the satellite in the southern hemisphere. The ninth orbit of the day passes far from the BMA zone.

Inspection of Fig. 4 reveals presence of third, additional inner radiation belt of the Earth magnetosphere at fourteen and thirty four minutes of flight (these minutes correspond to Mc-Ilwain parameter $L \approx 1.6$). The other, commonly known inner and outer Van-Allen radiation belts are pronounced for $L \approx 2.8$ on both hemispheres of the Earth. It is seen in Fig. 4 the particle intensity enhancement in all three belts around the time of weak geomagnetic storm of 8 May 2009. It was found from the extended analysis that for the Northern hemisphere the ratio of intensities in additional and main inner belts exceed unity in 25 occurrences from 31 for the electrons with energies $\Delta E = 0.18$ —0.51 MeV, and the ratio mentioned above less of unity in 26 occurrences from 31 for electrons with energies $\Delta E = 0.35—0.95$ MeV. The energy spectra in both inner belts differ strongly: a harder spectrum is seen in the "classical" Van-Allen belt in comparison with the third one appearing sporadically.

The third additional innermost belt was pronounced at locations rather far from the BMA zone, but inside the BMA itself too. This is well illustrated in Fig. 5 where the signal variations are plotted for orbit crossing the BMA. The horizontal axis covers a wide range of L-values of the Southern hemisphere. Plotted are observed dependence of the signal seen in 10 energy channels of D3, and in D4 detectors as recorded on 9 August 2009. Although the L—B coordinates are not strictly valid inside the BMA region it is useful in revealing presence of two zones inside the BMA region: the first one corresponds to domain with a wider shape along the L-coordinate, the one

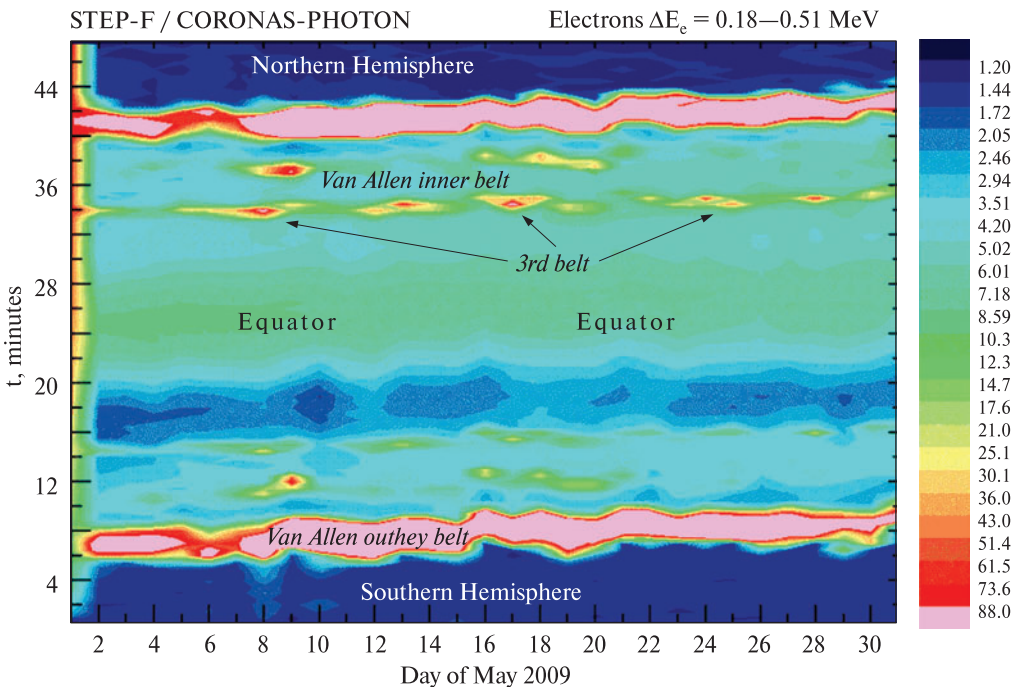

Fig. 4. Diagram showing time dependence of STEP-F signal for electrons of energies from the range $\Delta E_e = 0.18—0.51$ MeV. For every day in May 2009, the intensity is plotted as observed along the ninth ascending orbit of the day. Main features are identified. Weak geomagnetic storm took place on 8th May

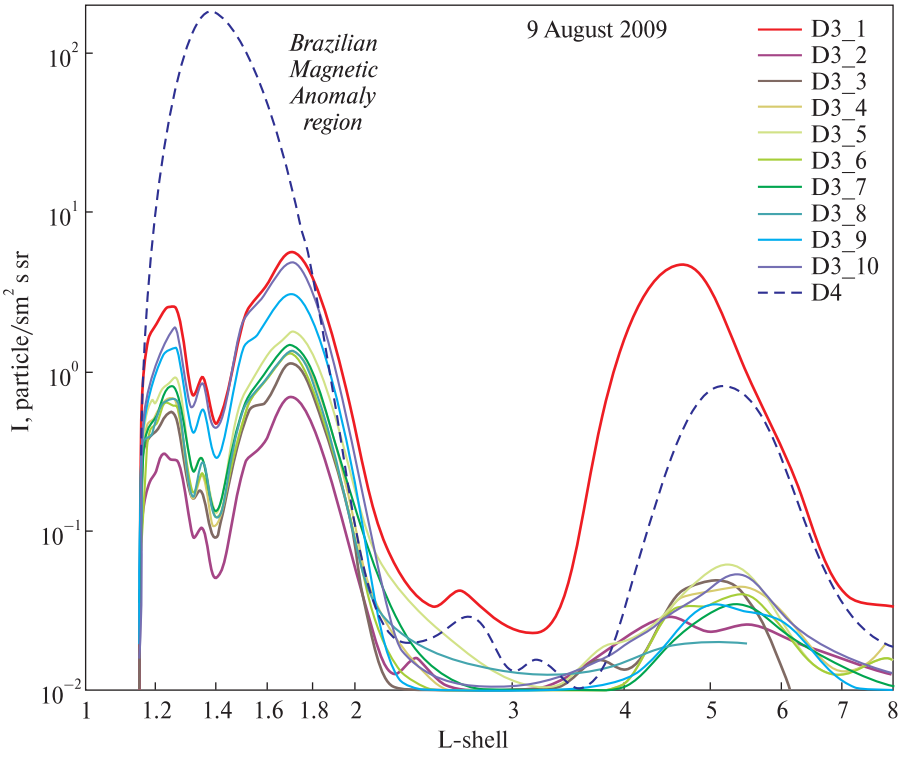

Fig. 5. L-dependence of the signals observed on 9 August 2009 in 10 energy channels from D3 detector data, and in detector D4. The orbit selected crosses the BMA as indicated

corresponds to the Van-Allen inner belt, and the second one of a narrower profile placed over smaller values along the L-coordinate. Such two-bump distribution is observed in all 10 energy channels of D3 detector recording channel but is not seen in the D4 detector records.

As it was mentioned above STEP-F detector D4 is sensitive to electrons with the energy from the range close to $E_{D4e} \approx 335$ keV. This explain straightforward the missing of two-bump character of the particle flux distribution in the D4 sensor channel as the electron spectrum falls off rapidly toward higher energies in the innermost (third) belt. As noted before, the STEP-F D3 detector is sensitive also to secondary γ-quanta, the source of which are primary electrons with energies $E_e \leq 0.3$ MeV. A single exclusion from this rule is for the energy channel D3_1 since it records electrons which passed the second D2 silicon matrix as evidenced by registration of outer belt electrons. As far as electron energy spectrum falls-off quickly in the outer radiation belt as compared with the spectrum inside the BMA, the number of measured γ-quanta at $L \approx 4$—6 is less by factor 10—100 in all energy ranges as it can be seen in Fig. 5.

Radial diffusion of intermediate energy electrons in the outer radiation belt

As far as the energy spectrum of electrons outside the BMA region is significantly softer than those in BMA, the values of E_{thr1}, E_{thr2}, and E_{D4e} for the Van Allen outer RB should be different than in the BMA. In order to determine the E_{thr1}, E_{thr2}, and E_{D4e} values, two approaches can be applied. The first one consists of plotting the dependence of L-shell averaged values, at which maximal values of particle fluxes in the outer RB were observed, as a function of their energy. It is known that the higher the energy of trapped particles, the deeper layers of the magnetosphere they drift on their way from one mirror point in polar oval of northern hemisphere to another magnetic mirror point in the southern hemisphere, and back. Having determined the values of L-shells from *Det1* and *Det2* detectors of the SphinX spectrophotometer and the D4 detector of the STEP-F telescope, and using the known dependence of the L-shells, at which maximal particle intensities of D1e, D2e, and D1p channels of the STEP-F device were recorded, we can estimate respective values of E_{thr1}, E_{thr2} and E_{D4e}.

The second approach consists of the determination of L-shells displacement ΔL, on which maximal values of electron fluxes were observed in geomagnetically quiet days before geomagnetic storm start, and in its recovery phase. The L-shell displacements occur due to electron radial diffusion on the Earth magnetic field jumps during the main phase of the storm development, and at the recovery phase initial stage of this storm. ΔL displacement is in inverse dependence to the primary electron energy. Having

determined ΔL from the data of *Det1*, *Det2* and D4 sensors, and comparing them with similar results of STEP-F instrument channels, the values of E_{thr1}, E_{thr2} and E_{D4e} can be estimated by this independent method.

Fig. 6 shows aligned results of the data analysis obtained from analysis of records obtained for ascending nodes of ninth orbit of the day in the Earth northern hemisphere. A significant variation of L-shell values (left-hand scale of the OY axis) is due to the weak magnetic storm occur in this period, and as a consequence, ΔL-displacement to the region of smaller L values due to radial diffusion of electrons crosswise the magnetic field lines. The statistical error of ΔL values (the right-hand scale of the vertical axis) cannot be determined because in the analysis the data from only one magnetic storm are available now. As a consequence, the graph has a small unphysical negative value $(\Delta L)_6 = -0.01$. Obviously, the values of ΔL, for which $\Delta L \geq 0.03$ holds true and are valid for the present analysis.

As a result, the inspection of both graphs in Fig. 6 provide the following values $E_{thr1} \approx 5$ keV, $E_{thr2} \approx$ ≈ 60 keV and $E_{D4e} \approx 240$ keV. As mentioned above, the *Det2* detector was additionally covered by the tantalum plate with a total thickness of 400 μm while maintaining an open detector window with the area of 4.9×10^{-3} cm^2. With such a thickness of the protective layer of material of the density $\rho = 16.65$ g/cm^3 and the charge $Z = 73$, electrons with energies $E_e \geq$ ≥ 1.2 MeV should reach the active layer of the detector. However, the protective layer itself is a good target for the secondary low energy gamma radiation generation as a result of irradiation by high energy primary electrons.

The E_{thr2} value in outer RB is less by factor ≈ 10 comparatively with that one in BMA region. It comes as a result of the soft character of electron spectrum in the RB. The E_{thr2} is reduced also as a part of the low energy electron fluxes enters directly through the detector window with an opening of area of $4.9 \times$ $\times 10^{-3}$ cm^2, subsequently recorded by the sensitive volume of the large area PIN photodiode. The contribution of direct detected electrons in the total counts of the *Det1* sensor is much higher, but the presence of very low-energy γ-quanta still may not be excluded because of substantial count rates in the narrow field of view.

E_{D4e} values for the BMA and outer RB don't differ strongly from each other due to specific selection logic mode in the channel D4e. The registration of events in this channel is carried out only in that case, when the desired signals have been observed simultaneously in all four layers of the STEP-FD detector head. It means that electrons producing secondary

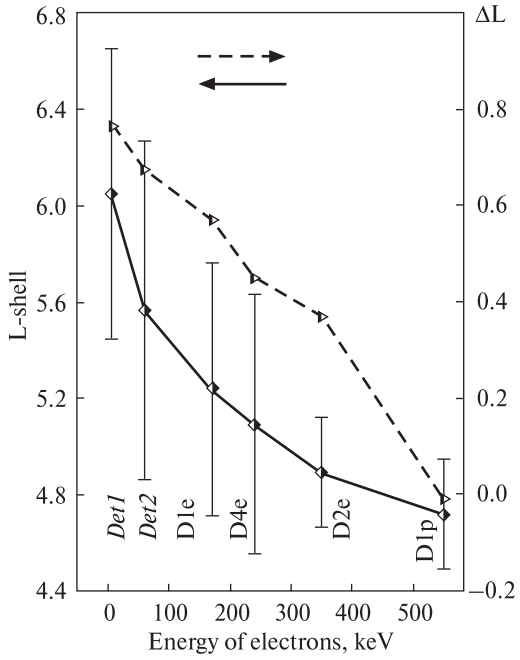

Fig. 6. The dependence of L-shell averaged values for the period of May 1—14, 2009, with maximal particle fluxes in the outer RB (left-hand vertical scale) on their energy for the ascending nodes of the ninth orbits of a day in the northern hemisphere (solid line). The dashed line shows the dependence of L-shell displacements with maximal particle fluxes (the right-hand scale of the vertical axis) inward the magnetosphere on the electron energy. The ΔL-displacement is the result of the radial diffusion process during the beginning stage of recovery phase of the weak geomagnetic storm on May, 9—11. As the start positions of L-shells period since 2nd to 3rd May was chosen before the storm. Horizontal arrows show the graphs belonging to the left-hand or right-hand scales

γ-quanta in the material of D3 scintillation detector, or the construction materials of the detector head, reach at least the second layer of position-sensitive silicon matrix sensors. At the same time, the decrease of the E_{D4e} value from ~335 keV for the BMA to ~240 keV for the RB also comes as a result of softening the particle energy spectrum in the RB, as compared with the shape of the electron spectrum in the BMA.

Evidence for anisotropic electron fluxes in the magnetospheric lower layers arising from interpretation of the STEP-F and SphinX data

Early inspection of the measurements from the analyzed instruments indicated for possible substantial anisotropy (beaming) of electron fluxes contained in the Van-Allen Belts. In order to verify this hypothesis we investigated dependences of particle intensity variations during the period between 1st and 14th May, 2009 on descending nodes of 13th orbits of the day (in UT). The variability patterns have been created for the D1e and D2e channels of the STEP-F device, and for the *Det1* and *Det2* signals

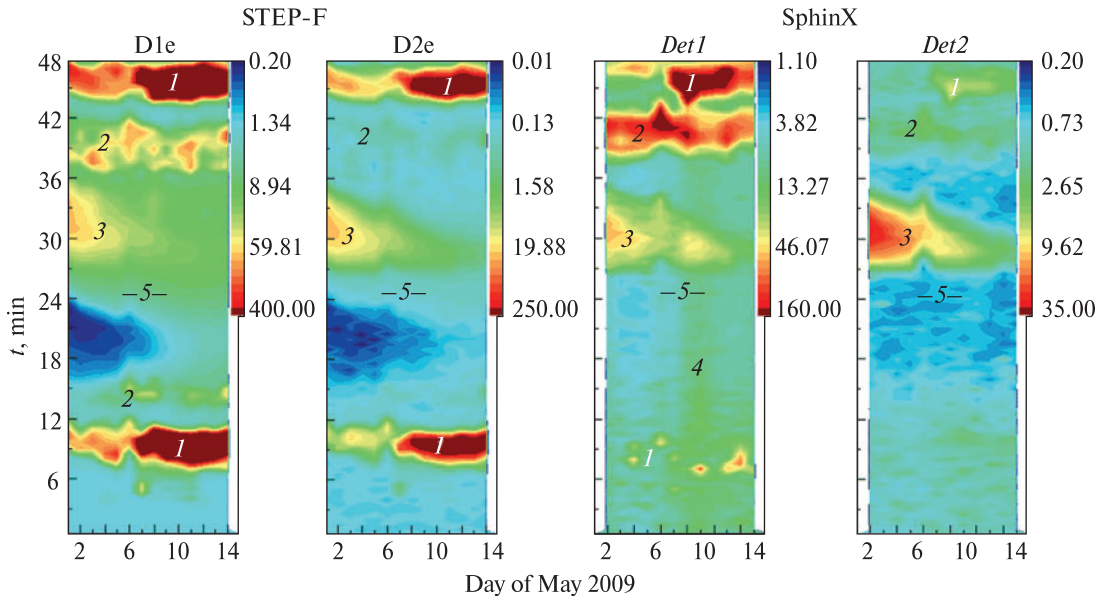

Fig. 7. Patterns of measured signal variations for period between May, 1 and May, 14, 2009 for STEP-F D1e and D2e detectors, and SphinX *Det1* and *Det2* sensors bottom to top descending nodes of 13th satellite orbits of the day as counted in UT is plotted for each calendar day. The annotated regions on the plots are: *1* — outer RB; *2* — inner RB; *3* — peripheral region of BMA; *4* — particles recorded by *Det1* sensor during the main phase of geomagnetic storm; *5* — geographic equator

of the SphinX instrument. We present the results in Fig. 7. Here, the time t is counted from the moment the satellite reach maximum northern elongation. Accordingly, the satellite passed through Van- Allen outer RB between 7th and ≈11th minute, and between 44th and ≈48th minutes (zone 1); the inner RB crossing took place between 15th and ≈38th (zone 2); the peripheral region of BMA (zone 3) was crossed around 42nd minute.

Fig. 7 clearly demonstrates almost identical detection levels of electron flux in both energy channels of the STEP-F instrument. At the same time the SphinX device did not measured any substantial particle fluxes in the northern hemisphere. However *Det1* saw substantial emission component while crossing the southern RB. The effect is also present for *Det2* to a smaller magnitude. Having in mind rather narrow directivity pattern for detection of particles by *Det1* and *Det2* detectors, such asymmetry in the responses on passage of the same radiation belt in different hemispheres tell us, on rather strong directivity for electrons contained in the RB.

In our opinion essential distinction in *Det1* and *Det2* sensor readouts as recorded by SphinX instrument during inner and outer RBs passages in the southern hemisphere of the Earth not corresponding to significant differences in STEP-F D1e and D2e readouts. Such behavior can be explained by preferable registration of secondary γ-radiation by both sensors of X-ray spectrophotometer. These γ-quanta have spectra steeply falling off with energy increasing. Having in mind that the response of D1e channel while crossing of southern Van-Allen inner belt was unnoticeable it can be concluded that the *Det1* sensor has confidently detected γ-quanta generated by primary electrons of energy, which should be of energy much lower than D1e threshold energy, i.e. $E_e << 180$ keV. This conclusion is supported by *Det1* sensor seeing precipitating electron fluxes in the time of the main phase of geomagnetic storm of May, 8, 2009 at all latitudes (zone 4) including the geographic equator (zone 5).

A gap filling between inner and outer RBs as well as a gap filling between the outer RB and plasmasphere boundary layer has been observed on many occasions before using omnidirectional detectors. In our case due to rather narrow fields of view of X-ray spectrophotometer sensors, and because of strongly beamed character of particle fluxes at the height of 550 km orbit, the gap filling between RBs in the southern hemisphere has not been detected.

At last, prominently observed by detector *Det2* peripheral area of the BMA (zone 3) provide supporting evidence for essential distinction in the character of electron energy spectra present inside the BMA and in the Earth RBs.

Acknowledgements

The research leading to these results was supported by the State Space Agency of Ukraine, State Contracts No. 1-22/05 and No. 1-04/08. The Science and Technology Center in Ukraine (STCU) has

supported this work too, Grant No. 1578. We also acknowledge financial support from the European Commission, Grant FP7/2007-2013: eHEROES, Project No. 284461.

REFERENCES

1. *Dudnik A.V., Persikov V.K., Zalyubovsky I.I., Timakova T.G., Kurbatov E.V. et al.* High Sensitivity STEP-F Spectrometer—Telescope for High-Energy Particles of the "CORONAS-Photon" Satellite Experiment // Solar System Research. — 2011. — V. 45. — No. 3. — P. 212—220.
2. *Dudnik O.V.* Dynamics of the Earth radiation belt electrons in May, 2009, on the base of the STEP-F instrument observations / In the book "Results of space experiment "CORONAS-Photon". Propositions on the continuation of "Coronas" program: scientific tasks and apparatus". ISSN 2075-6836. Series "Mechanics, operation and informatics". — 2012. — Moscow. — SRI RAS. — P. 103—125 (in Russian).
3. *Gburek S., Sylwester J., Kowalinski M., Bakala J., Kordylewski Z. et al.* SphinX soft X-ray spectrophotometer: science objectives, design and performance // Solar System Research. — 2011. — V. 45. — No. 3. — P. 189—199.
4. *Podgorski P., Dudnik O., Sylwester J., Gburek S.., Kowalinski M. et al.* Joint analysis of SphinX and STEP-F instruments data on magnetospheric electron flux dynamics at low Earth orbit / 39th Scientific Assembly of COSPAR (July 14-22, 2012, Mysore, India) Abstracts. Panel PSW.3: "Space Weather Data: Observations and Exploitation for Research and Applications". — STW-C-119 PSW.3-0028-12. — P. 112.
5. *Dudnik O., Podgorski P., Sylwester J., Gburek S., Kowalinski M., Siarkowski M., Plocieniak S., Bakala J.* X-Ray Spectrophotometer SphinX and Particle Spectrometer STEP–F of the Satellite Experiment "CORONAS-Photon". Preliminary Results of the Joint Data Analysis // Solar System Research. — 2012. — V. 46. — No. 2. — P. 160—169.
6. *Dudnik O.* Unexpected behavior of subrelativistic electron fluxes under Earth radiation belts / 4th International workshop HEPPA/SOLARIS—2012 (9—12 October 2012, Boulder, Colorado, USA). — Abstract book. — P. 15.
7. *Dudnik O.V.* Observations of three electron radiation belts in the Earth' magnetosphere on the data of the STEP-F device on board the "CORONAS-Photon" spacecraft / 12th Ukrainian conference on space research (3—7 September 2012, Yevpatoria, Crimea, Ukraine) Abstracts. — P. 70 (in Russian).
8. *Dudnik O., Sylwester J., Podgórsi P., Gburek S.* Radiation belts of the Earth: overview, methods of investigations, recent observations on the "CORONAS-Photon" spacecraft / Conference "Progress on EUV&X-ray spectroscopy and imaging" (20-22 November 2012, Wroclaw, Poland). Abstracts. — P. 3.